

pubs.acs.org/NanoLett Letter

# pH-Mediated Mucus Penetration of Zwitterionic Polydopamine-Modified Silica Nanoparticles

Yubin Ma, Yiyang Guo, Shan Liu, Yu Hu, Cheng Yang, Gang Cheng, Changying Xue, Yi Y. Zuo, and Bingbing Sun\*



Cite This: Nano Lett. 2023, 23, 7552-7560



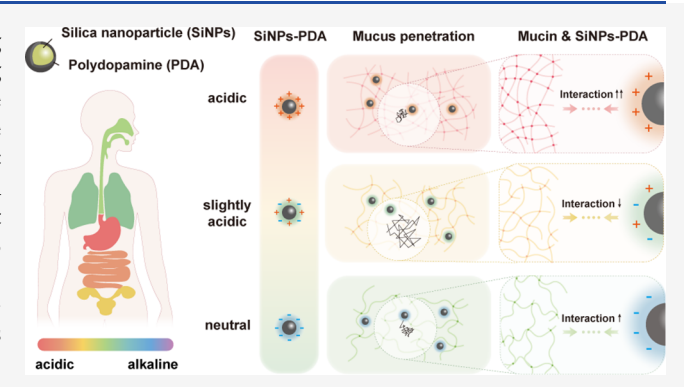
**ACCESS** I

Metrics & More

Article Recommendations

s Supporting Information

ABSTRACT: Zwitterionic polymers have emerged as promising trans-mucus nanocarriers due to their superior antifouling properties. However, for pH-sensitive zwitterionic polymers, the effect of the pH microenvironment on their trans-mucus fate remains unclear. In this work, we prepared a library of zwitterionic polydopamine-modified silica nanoparticles (SiNPs-PDA) with an isoelectric point of 5.6. Multiple-particle tracking showed that diffusion of SiNPs-PDA in mucus with a pH value of 5.6 was 3 times faster than that in mucus with pH value 3.0 or 7.0. Biophysical analysis found that the trans-mucus behavior of SiNPs-PDA was mediated by hydrophobic and electrostatic interactions and hydrogen bonding between mucin and the particles. Furthermore, the particle distribution in the stomach, intestine,



and lung demonstrated the pH-mediated mucus penetration behavior of the SiNPs-PDA. This study reveals the pH-mediated mucus penetration behavior of zwitterionic nanomaterials, which provides rational design strategies for zwitterionic polymers as nanocarriers in various mucus microenvironments.

KEYWORDS: zwitterionic polymer, polydopamine, mucus penetration, pH microenvironment

he mucus lining on the mucosal surface works as a natural barrier against the invasion of pathogens. However, the existence of mucus hinders the trans-mucus delivery of medications, resulting in a low administration efficiency and poor bioavailability. 1,2 To facilitate efficient diffusion of payload molecules through mucus, various strategies have been designed.<sup>3,4</sup> Among the numerous mucus-penetrating materials, zwitterionic polymers have been attracting attention in recent years. Their superior antifouling property to resist mucin, which is the major protein component of the mucus blanket, is considered as a critical factor for zwitterionic nanoparticles (NPs) to penetrate readily through the mucus barrier. As the representative zwitterions, betaine-based<sup>7-10</sup> and phosphorvlcholine-based<sup>11,12</sup> polymers have been applied in mucosal drug delivery, enabling particles to penetrate across both mucus and epithelial barriers.

The conventional zwitterionic unit contains a permanent positively charged quaternary amine and a negatively charged group to maintain an overall zwitterionic state under most physiological conditions. However, the weak zwitterionic behaviors caused by various pH environments have been observed in certain zwitterionic polymers, e.g., the poly-(carboxybetaine)-based polymer, polydopamine, 15,16 and amino acid-derived polymers. The pH condition significantly affects their characteristics, e.g., surface charge, 15,18 surface

hydrophobicity, 19,20 and antifouling performance. 17,18 When they are delivered to various mucosal tissues, the pH-sensitive behaviors of zwitterionic polymers were noted due to a wide-pH range microenvironment of mucus. 21,22 The mucus layer is approximately neutral in the airways  $(pH \sim 7.1)^{23}$  and eyes  $(pH \sim 7.1)^{23}$  $\sim$ 7.3) $^{22,24}$  of humans. Along the gastrointestinal tract, the mucus pH increases from harsh acidic in the stomach<sup>25</sup> to slightly acidic or neutral in the small intestine (pH 5.0-7.5).<sup>26</sup> Additionally, the mucus pH of the cervix ranges from slightly acidic to basic (pH 5.4–8.2) with the menstrual cycle. 22 Thus, the pH-sensitive zwitterionic materials could exhibit the desired mucus penetrability in a targeted mucus microenvironment, which further determines their applicability as trans-mucus delivery vehicles. However, there has been no systematic study of the effect of pH on the mucus penetrability of zwitterionic NPs and the underlying mechanism.

In this work, using PDA as a representative pH-sensitive zwitterionic material, we investigated the effect of pH on the

 Received:
 June 6, 2023

 Revised:
 July 12, 2023

 Published:
 July 26, 2023





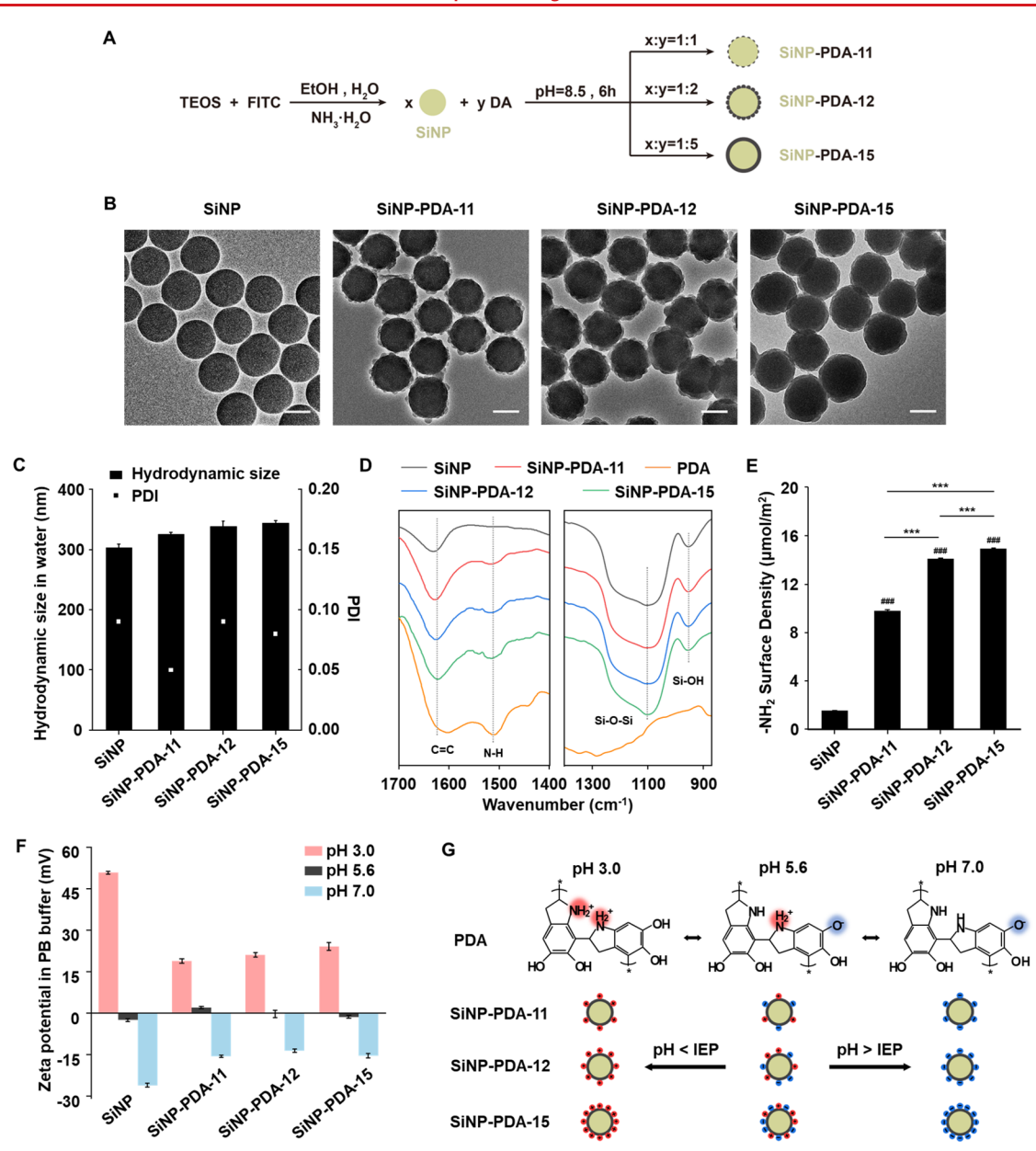


Figure 1. Schematic illustration and characterization of NPs. (A) Schematic representation of the synthesis routes of pristine SiNPs and SiNPs-PDA with different ratios of SiNPs and DA. (B) Representative TEM images of SiNPs and SiNPs-PDA. The scale bar is 200 nm. (C) Hydrodynamic sizes and polydispersity indices (PDI) of the particles in water. (D) FTIR spectra of SiNPs, SiNPs-PDA, and PDA. The N–H symmetrical bending vibration (δ N–H, 1510 cm<sup>-1</sup>), C=C stretching vibrations of conjugated aromatic rings ( $\nu_{C=C}$ , 1620 cm<sup>-1</sup>), Si–O–Si asymmetric stretching vibration ( $\nu_{Si-O-Si}$ , 1100 cm<sup>-1</sup>), and Si–OH stretching vibration ( $\nu_{Si-OH}$ , 955 cm<sup>-1</sup>) were identified. (E) Quantification of PDA on the surface of SiNPs-PDA by measuring the density of amine groups using an acid orange analysis. (F)  $\zeta$  potentials of particles in 10 mM of PB with different pH values. (G) Schematic illustration of the pH-dependent structure of PDA and surface charge of PDA-modified SiNPs. \*\*\*p < 0.001 and \*##p < 0.001 compared to SiNPs.

mucus penetration behavior of PDA-modified silica NPs. A library of NPs were prepared to determine the differential mucus penetration behavior when pH was less than, equal to, and greater than their IEP at 5.6, mimicking the different local mucus microenvironments of the body. Furthermore, the surface properties of NPs, the microstructure of the mucin polymer, and the interaction between them were investigated in different pH environments. The *in vivo* distribution model further demonstrated the pH-mediated trans-mucus fate of zwitterionic particles. This study provides a better understanding of the application of zwitterion-based carriers in mucosal drug delivery.

Due to the size exclusion effect of mucus, NPs with a diameter of 200–500 nm more easily penetrate the mucus layer. <sup>27,28</sup> Therefore, 300 nm FITC-labeled pristine SiNPs were synthesized by using the Stöber method. Polymerized dopamine (DA) was grafted onto SiNPs to form a layer of zwitterionic polydopamine. With an increase in the mass of PDA grafted on SiNPs, a library of SiNPs-PDA with different Si:DA ratios were prepared, and they were noted as SiNPs-PDA-11, SiNPs-PDA-12, and SiNPs-PDA-15 (Figure 1A). Transmission electron microscopy (TEM) images showed that pristine SiNPs were spherically shaped with diameters of ~300 nm, and the coating became complete and smoother with the DA:Si ratio increasing

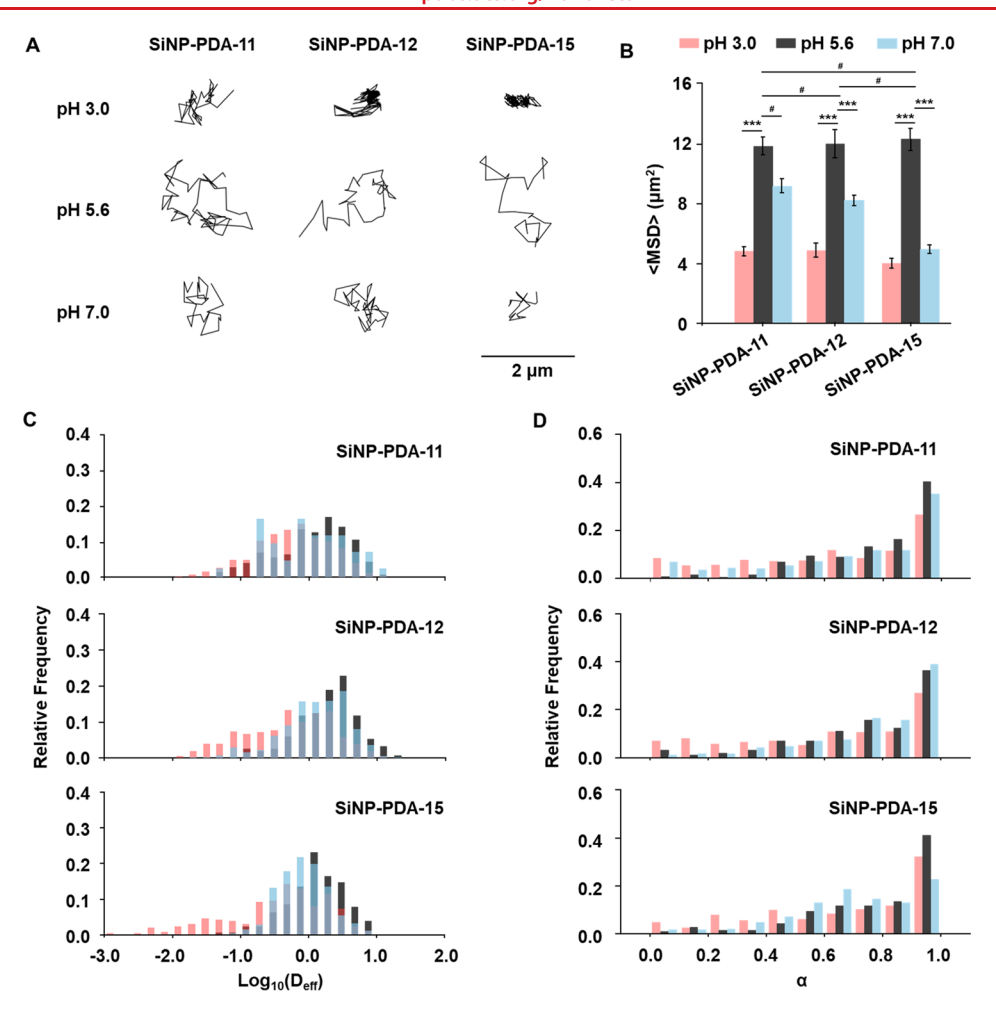


Figure 2. Determination of the mucus penetration ability of SiNPs-PDA by MPT. (A) Representative trajectories, (B) ensemble mean squared displacement ( $\langle MSD \rangle$ ), (C) distribution of the logarithms of effective diffusivities ( $D_{\rm eff}$ ), and (D) anomalous exponents ( $\alpha$ ) of SiNPs-PDA in reconstituted mucus with pH values of 3.0, 5.6, and 7.0. Data represent means  $\pm$  the standard error of the mean. \*\*\*p < 0.001. The time scale is 1 s.

from 1:1 to 5:1 (Figure 1B and Figure S1). The dynamic light scattering (DLS) analysis showed that the hydrodynamic size of SiNPs was  $303 \pm 6$  nm with a good monodisperse distribution (PDI = 0.09) in water (Figure 1C). With the increase in the PDA on SiNPs, the hydrodynamic sizes were gradually increased to  $326 \pm 2$ ,  $339 \pm 8$ , and  $344 \pm 4$  nm, respectively. Fourier transform infrared spectroscopy (FTIR) was used to determine the surface functional groups (Figure 1D). The increased intensity of N-H and C=C vibration bands indicated the presence of the amine group and benzene ring of PDA on SiNPs-PDA. With an increase in the DA:Si ratio, the mass of surface PDA increased, which was further confirmed by the thermogravimetric analysis (TGA) (Figure S2). The density of amine was quantified using acid orange analysis, confirming the number of functional groups on the surface increased with an increase in the DA:Si ratio (Figure 1E). 29,30 The trace amount of -NH<sub>2</sub> on pristine SiNPs was possibly caused by the addition of APTEs during the synthesis of SiNPs.

The  $\zeta$  potentials of SiNPs at pH values of 3.0, 5.6, and 7.0 were 51, -2, and -26 mV, respectively. Due to the presence of small amounts of amine groups, the IEP of FITC-labeled SiNPs was higher than that of silica without labeling, which was ~2.5<sup>31</sup> (Tables S1 and S2). After PDA modification, the  $\zeta$  potentials of particles were approximately 20, 0, and -15 mV at pH values of 3.0, 5.6, and 7.0, respectively (Figure 1F), and there was no significant difference in  $\zeta$  potentials among SiNPs-PDA with

different PDA densities. The isoelectric point (IEP) measurement showed that SiNPs-PDA-15 exhibited IEPs of 5.6 (Figure S3). It has been generally accepted that the monomer contains a great amount of amino and phenolic hydroxyl groups. <sup>32,33</sup> Thus, a proposed structure was used to describe the pH sensitivity of PDA (Figure 1G). When the pH was below their IEP, the protonation of amino groups predominated over the deprotonation of phenolic groups, leading to the cationic state of SiNPs-PDA. <sup>34</sup> In comparison, SiNPs-PDA showed charge balance when the pH was equal to their IEP and possessed anionic character when the pH was above their IEP. It was noted that the balanced (under pH 5.6) or unbalanced (under pH 3.0 and 7.0) surface charge in different pH environments was amplified with an increase in PDA density (Figure 1G).

The diffusion behavior of PDA-modified NPs in mucus was further investigated. The pH of reconstituted mucus was adjusted from acidic to neutral to mimic the pH microenvironment in different mucosal tissues, and multiple-particle tracking (MPT) was used to determine the motility behavior of particles. The elucidation of mucus-penetrating behavior of the nanocarrier by using the artificial mucus model based on commercial mucin has been accepted. The movement of SiNPs-PDA was displayed visually by representative trajectories and movies (Figure 2A and Movie S1). It was shown that the SiNPs-PDA diffused freely at pH 5.6 and were restricted significantly as the mucus became acidic (pH 3.0) or neutral

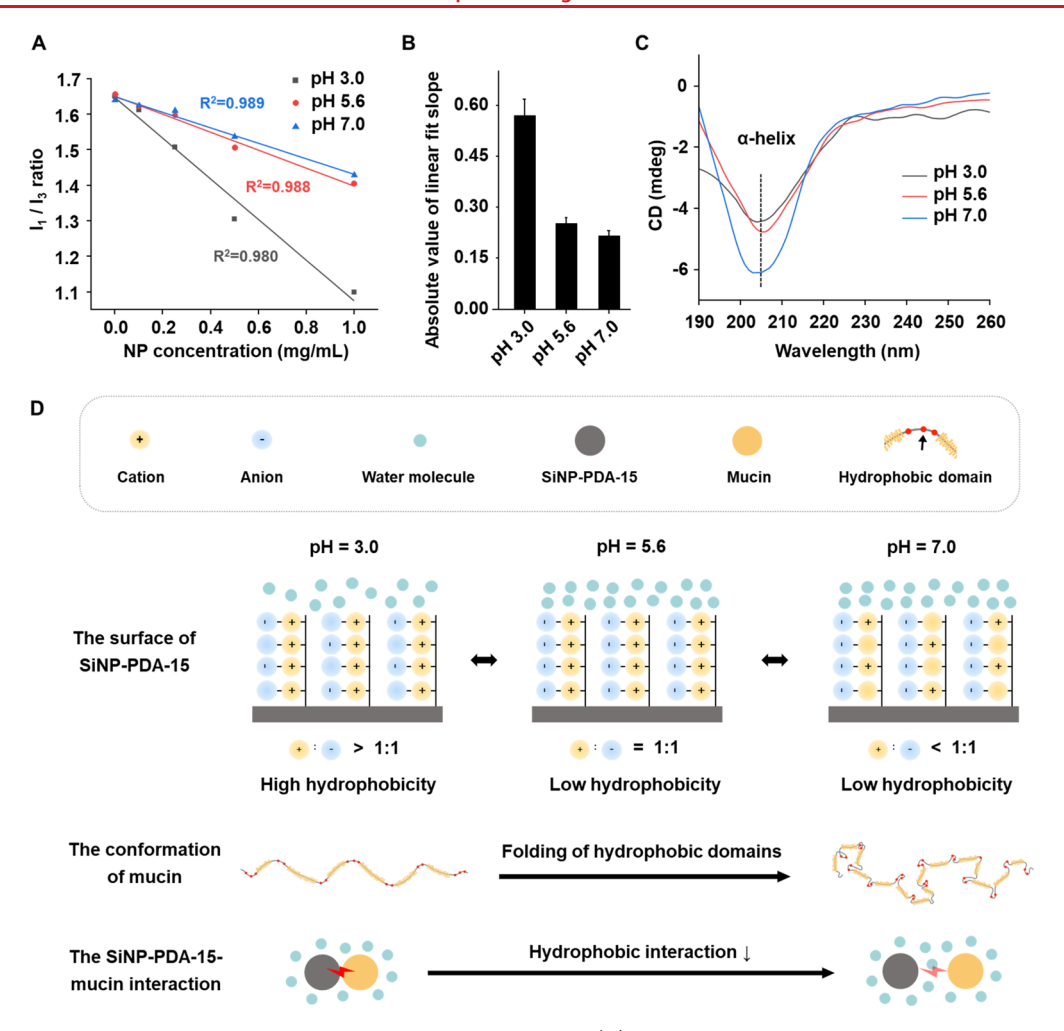


**Figure 3.** Hydrophobicity of SiNPs-PDA-15 and mucin at different pH values. (A)  $I_1/I_3$  ratio of pyrene as a function of NP concentration under different pH conditions. (B) Hydrophilicity of SiNPs-PDA-15 determined by calculating the slope of the linear fit of the  $I_1/I_3$  ratio vs the NP concentration. (C) CD spectra of mucin in 10 mM of PB at different pH values. (D) Schematic representation of the pH-dependent hydrophobicity of both SiNPs-PDA-15 and mucin and the proposed NP-mucin hydrophobic interaction.

(pH 7.0). The ensemble mean squared displacement ( $\langle MSD \rangle$ ) was calculated to evaluate the diffusion ability of NPs (Figure 2B). The SiNPs-PDA-11, SiNPs-PDA-12, and SiNPs-PDA-15 all exhibited maximum (MSD) values (11.80, 11.95, and 12.8  $\mu$ m<sup>2</sup>, respectively) in mucus at pH 5.6. This indicated that the balanced charges on SiNPs-PDA, even in a small amount, provided particles with good penetration ability. When the mucus pH was changed to 3.0 or 7.0, the (MSD) values were reduced. This reduction was augmented by the increase in PDA density, reaching 3.1 and 2.5 times for SiNPs-PDA-15 at pH values of 3.0 and 7.0, respectively. This suggested that the pHmediated mucus penetrability of SiNPs-PDA became more significant with an increase in unbalanced positive and negative charges on the particle surface. The logarithms of the effective diffusion coefficient  $(D_{\rm eff})$  were further calculated, which demonstrated higher transport rates of SiNPs-PDA at pH 5.6 than at 3.0 and 7.0 (Figure 2C). The anomalous exponent ( $\alpha$ ) represents the extent of being restricted for NPs in mucus, and a higher  $\alpha$  value means less trapping of NPs in mucus. The value of 0.5 was chosen as the cutoff to further identify whether the NPs were trapped ( $\alpha$  < 0.5) or diffusive ( $\alpha$  > 0.5). <sup>39</sup> For SiNPs-PDA-15, 31%, 12%, and 18% were trapped in mucus with pH values of 3.0, 5.6, and 7.0, respectively (Figure 2D). In comparison, pristine SiNPs exhibited a lower (MSD) of 0.56  $\mu$ m<sup>2</sup> in mucus

with a pH value of 5.6 compared with values of 4.92 and 6.34  $\mu$ m<sup>2</sup> in mucus at pH 3.0 and 7.0, respectively (Figure S4). This can be explained by the fact that SiNPs barely carry charge at IEP, whereas SiNPs-PDA show a zwitterionic surface. The uncharged surfaces may form more hydrogen bonds with mucin, <sup>25</sup> limiting their trans-mucus capability. Altogether, the SiNPs-PDA showed the optimized diffusion behavior in mucus with a pH value of 5.6, and this diffusion behavior was weakened when pH values were greater or less than their IEPs.

The viscosity of reconstituted mucus with different pH values was characterized, which showed a typical shear-thinning behavior as the viscosity decreased with an increase in shear rate (Figure S5). The enhanced adhesion caused by the increasing viscosity of mucus in an acidic environment has been well-documented, <sup>25,35</sup> which may provide us with a potential explanation for SiNPs-PDA's poor transportation performance at pH 3.0. However, the pH-dependent mucus viscosity alone cannot provide a convincing explanation for the complex process of mucus penetration of NPs at higher pH values. Thus, a series of biophysical characterizations were used to further analyze this process. As the major protein in mucus, the mucin is entangled and forms a dense fiber mesh that protects against the diffusion of foreign particles.<sup>40</sup> The particle—mucin interaction has been demonstrated as a key

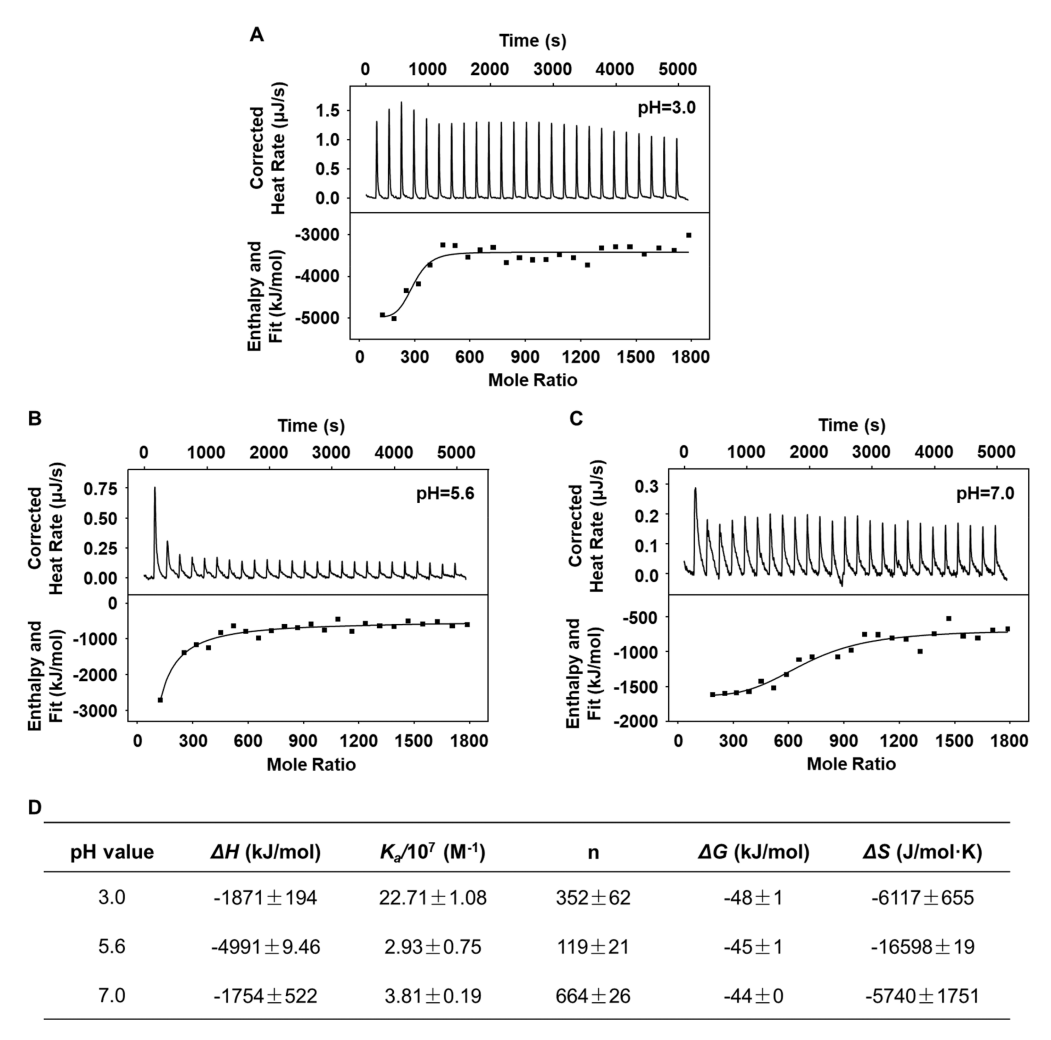


**Figure 4.** ITC analysis of the titration of mucin to SiNPs-PDA-15 in 10 mM of PB at pH values of (A) 3.0, (B) 5.6, and (C) 7.0. The top panel shows the corrected heat flow vs time during the injection of mucin over SiNPs-PDA-15; the bottom panel shows the heat generated from each injection vs the ratio of mucin and SiNPs-PDA-15, and the binding curve is fitted by an independent model. (D) Thermodynamic parameters were calculated by an independent model from the titration of mucin to SiNPs-PDA-15 in 10 mM of PB at 25 °C and pH 3.0, 5.6, and 7.0.

parameter in determining the mucus penetrability of particles. 21,41 Therefore, the affinity between particles and mucin was characterized by their co-incubation at different pH values. 36,42 The SiNPs-PDA-15 with the most significant pHmediated penetrability were used for the following analysis. After the SiNPs-PDA-15 and mucin had been mixed at various ratios (S:M) in buffer at different pH values, the sizes and  $\zeta$ potentials of particle-mucin complexes were determined (Figure S6). 43,44 Under slightly acidic conditions (pH 5.6), the maximum value of the complex size was  $807 \pm 55$  nm, showing a smaller complex compared to those at pH values of 3.0 (1637  $\pm$  27 nm) and 7.0 (1524  $\pm$  26 nm). This suggested that the adsorption of mucin on the particle surface was weak at pH 5.6 and stronger at pH 3.0 and 7.0. Additionally, the  $\zeta$ potential of the complex changed according to the ratio of SiNPs-PDA-15 to mucin, demonstrating the adsorption of more mucin to SiNPs-PDA-15 with an increase in the level of mucin in the complex. The larger  $\zeta$  potential difference between positively charged NP and slightly negatively charged mucin at pH 3.0 may result in stronger electrostatic interaction.

Furthermore, the interaction between SiNPs-PDA and mucin was systematically analyzed in terms of the surface properties of NPs to determine the underlying mechanisms that lead to the

different NP-mucin affinity and trans-mucus fate of NPs. Among the surface properties, the hydrophobicity of particles is a key factor. <sup>22</sup> For NPs in mucus, the highly hydrophobic surface could typically lead to a trapped state by mucin due to hydrophobic interaction. 45 Thus, the hydrophobicity of SiNPs-PDA-15 at different pH values was determined. Due to the different surface charges of SiNPs-PDA-15 under various pH conditions, pyrene, a non-ionic dye, was used for the hydrophobicity measurement. The fluorescence intensities at 370 nm  $(I_1)$  and 381 nm  $(I_3)$  were recorded using the fluorescence spectrophotometer, and the  $I_1/I_3$  ratios at various NP concentrations and different pH values were calculated (Figure 3A). In the pyrene assay, a lower  $I_1/I_3$  ratio indicates that the NPs are more hydrophobic. 46,47 Under all of the tested concentrations, the smaller  $I_1/I_3$  values at pH 3.0 indicated the higher hydrophobicity of NPs. With an increase in the NP concentration, the  $I_1/I_3$  ratios decreased, suggesting that SiNPs-PDA-15 changed the hydrophobic microenvironment in which pyrene was located. There was no significant difference in the  $I_1$ / I<sub>3</sub> ratio in buffers with different pH values, confirming the change in  $I_1/I_3$  was induced by the particles rather than the pH of the buffer. The slope of the linear fit of the  $I_1/I_3$  ratio against NP concentration was further calculated to quantify the hydro-

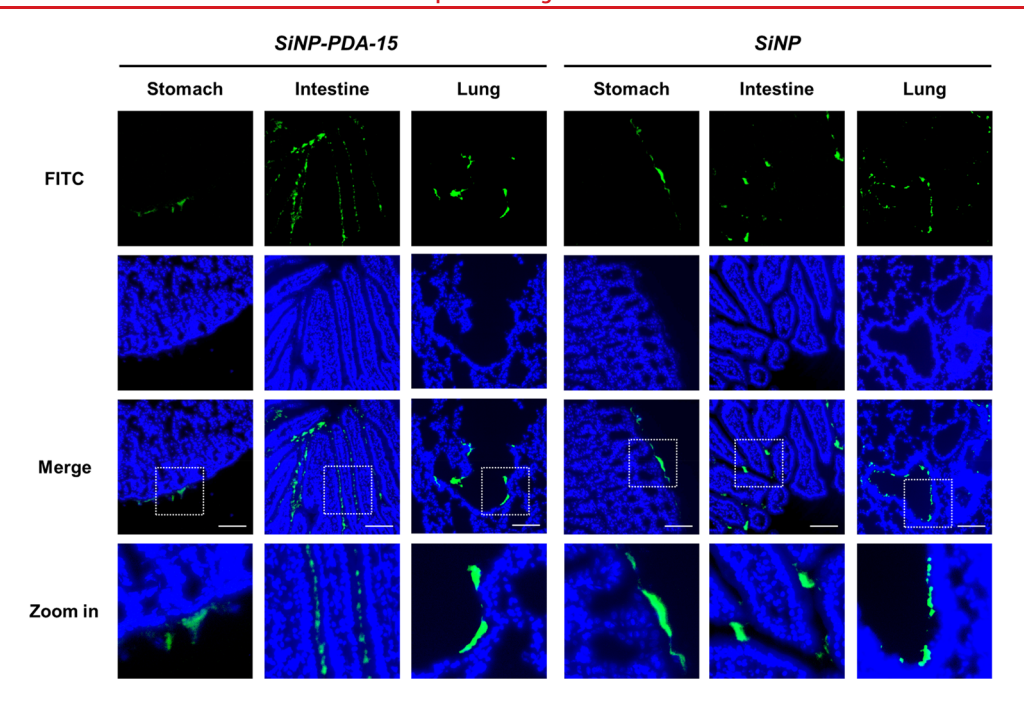


**Figure 5.** Distribution of SiNPs-PDA-15 and SiNPs in the stomach, intestine, and lungs of mice. One hundred micrograms of FITC-labeled SiNPs-PDA-15 or SiNPs was administrated to the stomach, intestine, and lung of mice via gavage, intestinal loop injection, and intratracheal instillation, respectively. NPs that accumulated around different mucosal surfaces were examined using a fluorescent inverted microscope. The SiNPs-PDA-15 and SiNPs were labeled with FITC (green). Cell nuclei were labeled with Hoechst 33342 (blue). The scale bar is  $100 \, \mu \text{m}$ .

phobicity of SiNPs-PDA-15 (Figure 3B). The slope value at pH of 3.0 was  $\sim$ 2.3-fold higher than those at pH 5.6 and 7.0. It has been reported that the ordering of water molecules around cations is much weaker than that around anions; thus, the pHinduced unbalanced charge of the zwitterionic polymer could weaken the hydrogen bond of the interfacial water. 14,48 The higher hydrophobicity of SiNPs-PDA-15 at a pH value of 3.0 was possibly attributed to weak water binding of the positively charged surface in a low-pH environment. The pH-dependent hydrophobicity of NPs was further confirmed by using the Nile blue (NB) dye adsorption method (Figure S7). Additionally, The environmental pH values could influence the stability of salt bridges between -COOH and -NH2 in mucin, leading to the different extent of conformational unfolding. 49 It was shown that the peak representing the  $\alpha$ -helix in the circular dichroism (CD) spectrum was weakened and widened with a decrease in pH (Figure 3D). The conformation of mucin was changed from a random coil to a rod shape, <sup>49,50</sup> which corresponded to the size change of 195  $\pm$  3 nm (pH 7.0) to 405  $\pm$  21 nm (pH 3.0), respectively (Figure S6A). With the unfolding of the glycosyl side chain, the hydrophobic regions were gradually exposed 49,50 and the hydrophobicity of mucin was increased. 51,52 Altogether, the higher hydrophobicity of both mucin and SiNPs-PDA-15 might lead to the strong hydrophobic interaction at pH 3.0.<sup>45</sup> In contrast, the hydrophobic interaction was weakened when the hydrophobicity of the mucin or NPs decreased at pH values of 5.6 and 7.0 (Figure 3D).

Additionally, the neutral surface charge is another favorable property for NPs to penetrate through mucus by weakening the electrostatic interaction with the negatively charged mucin. <sup>22,45</sup> Herein, the type and strength of particle—mucin interaction at the molecular level were investigated using isothermal titration calorimetry (ITC) analysis (Figure 4). <sup>35,53</sup> Generally, the particle—protein binding was a complex process involving two simultaneous processes, i.e., the exothermic formation of a

noncovalent bond and endothermic solvent reorganization.  $^{\rm 54,55}$ The interactions were exothermic and entropy loss processes, indicating that the interaction was an enthalpy-driven process (Figure 4D). The intense exothermic process was considered to be caused by the strong polymer-mucin interactions and the formation of noncovalent bonds, e.g., electrostatic interactions and hydrogen bonds. 56,57 The entropy loss during the adsorption process was possibly induced by conformational constraints and the loss of rotational freedom of the mucin. 56 Notably, the association constant  $(K_a)$  of  $2.93 \times 10^7 \,\mathrm{M}^{-1}$  at a pH value of 5.6 was  $\sim$ 7.7 and  $\sim$ 1.3 times lower than that at pH values of 3.0 and 7.0, respectively, and the number of adsorption sites (n) for SiNPs-PDA-15 at pH 5.6 was smaller than that at pH 3.0 and 7.0. This suggested that the mucin-SiNPs-PDA-15 interaction was weaker at pH 5.6 than at pH 3.0 and 7.0, which was consistent with MPT analysis (Figure 2). The lower particle-mucin affinity at pH 5.6 might be associated with weaker electrostatic interaction between neutral SiNPs-PDA-15 and negatively charged mucin (Figure S6B). Interestingly, for NPs at a pH value of 5.6, with a decrease in adsorptive strength, the heat release  $(\Delta H)$  and entropy loss  $(\Delta S)$  were significantly decreased. This might be due to the low degree of desolvation of SiNPs-PDA-15 caused by weak NP-mucin interaction. Fewer water molecules and ions on the surface of NPs were released at pH 5.6, leading to a smaller compensation for the loss of conformational entropy and the heat release during mucin binding.53

Additionally, the formation of hydrogen bonds between SiNPs-PDA-15 and mucin was confirmed by the blue shift of the mucin peak in the amide I region after adsorption on particles using FTIR analysis (Figure S8).<sup>58</sup> The peak shift was more significant with an increase in pH, which suggested that the stronger hydrogen bonding between -NH- in SiNPs-PDA-15 and -COOH or -OH in mucin might dominate over electrostatic interaction.<sup>59</sup> Altogether, this suggested that the interaction

between SiNPs-PDA-15 and mucin involves hydrophobic, electrostatic, and hydrogen bond interactions, which were responsible for the mucus filtration effects. Thus, during the design of the trans-mucus materials, the surface properties of NPs in the targeted mucus microenvironment should be considered to ensure optimized delivery. Admittedly, polydopamine could not represent the behavior of all zwitterions; it bears a large number of groups that can be protonated and/or deprotonated, which is consistent with the properties of numerous zwitterionic polymers. 14,17,19 Additionally, the mechanism of NP—mucin interaction also correlates well with the pH-sensitive antifouling ability of zwitterionic polymers. 18

On the basis of the in vitro results and mechanistic analysis presented above, the pH-mediated mucus penetration behavior of SiNPs-PDA-15 was further evaluated in vivo. The stomach and airway were covered by acidic and neutral mucus, respectively. The intestinal mucus of mice is slightly acidic  $(5.24 \pm 0.2 \text{ in the ileum})$ , lower than that of neutral pH in humans. 60,61 These mucosal tissues with different pH microenvironments were selected to study the particle distribution (Figure 5 and Figure S9). 37,62,63 The suspension of FITClabeled NPs was administrated to the stomach, intestine, and lungs of mice by gavage, intestinal loop injection, and intratracheal delivery, respectively. For intestinal distribution, the intestinal loop model was used instead of gavage to avoid the influence of the trans-gastric process on the distribution of NPs in intestinal mucus. SiNPs-PDA-15 were diffused deeper into the intestinal villi and evenly distributed along the mucus layer. In contrast, SiNPs-PDA-15 sparsely and discontinuously accumulated on the surface of the stomach and airway, respectively. Together with the in vitro results, this further demonstrated that the SiNPs-PDA-15 tended to diffuse better in slightly acidic mucus but were trapped or removed in acidic and neutral mucus (Figure 2). Additionally, the distributions of SiNPs in the mucus of different tissues were examined as a control. The poor distribution of SiNPs in slightly acidic intestinal mucus compared to that of those in the mucus of the stomach and airway was consistent with the MPT analysis (Figure S4).

In this paper, we demonstrated the pH-mediated mucus penetration capability of zwitterionic polydopamine-coated silica nanoparticles. When the IEP of NPs was equal to the pH value of the mucus microenvironment, the NPs exhibited superior diffusional transportation in both *in vitro* and *in vivo* models. Further biophysical analysis revealed that when the IEP of SiNPs-PDA matched the pH of the microenvironment, it resulted in lower particle—mucus affinity, thus the unhindered behavior of SiNPs-PDA in mucus. This study reveals the significance of matching the charge balance state with the mucus pH microenvironment for efficient trans-mucus delivery of pH-sensitive zwitterionic NPs. This provides a rational design strategy for zwitterionic materials as biomedicine and vaccines for targeted mucosal microenvironments.

#### ASSOCIATED CONTENT

# **Solution** Supporting Information

The Supporting Information is available free of charge at https://pubs.acs.org/doi/10.1021/acs.nanolett.3c02128.

Materials and methods; TEM images, TGA and IEP determination of SiNPs and SiNPs-PDA; hydrodynamic sizes and  $\zeta$  potentials of FITC-labeled and unlabeled SiNPs; MPT analysis of SiNPs; viscosity measurement of

reconstituted mucus; size and  $\zeta$  potential of the SiNPs-PDA/mucin mixture; hydrophobicity measurement using dye NB; ATR-FTIR spectra of adsorbed mucin; and *in vivo* distribution of particles (PDF)

Movie showing the motion of particles in mucus with different pH values (MP4)

#### AUTHOR INFORMATION

# **Corresponding Author**

Bingbing Sun — State Key Laboratory of Fine Chemicals, Dalian University of Technology, 116024 Dalian, China; School of Chemical Engineering, Dalian University of Technology, 116024 Dalian, China; Frontiers Science Center for Smart Materials Oriented Chemical Engineering, School of Chemical Engineering, Dalian University of Technology, Dalian 116024, China; orcid.org/0000-0002-5444-5078; Email: bingbingsun@dlut.edu.cn

#### **Authors**

Yubin Ma — State Key Laboratory of Fine Chemicals, Dalian University of Technology, 116024 Dalian, China; School of Chemical Engineering, Dalian University of Technology, 116024 Dalian, China; Frontiers Science Center for Smart Materials Oriented Chemical Engineering, School of Chemical Engineering, Dalian University of Technology, Dalian 116024, China

Yiyang Guo — State Key Laboratory of Fine Chemicals, Dalian University of Technology, 116024 Dalian, China; School of Chemical Engineering, Dalian University of Technology, 116024 Dalian, China; Frontiers Science Center for Smart Materials Oriented Chemical Engineering, School of Chemical Engineering, Dalian University of Technology, Dalian 116024, China

Shan Liu – School of Chemical Engineering, Dalian University of Technology, 116024 Dalian, China

Yu Hu – School of Chemical Engineering, Dalian University of Technology, 116024 Dalian, China

Cheng Yang — School of Chemistry, Dalian University of Technology, 116024 Dalian, China

Gang Cheng — Department of Chemical Engineering, University of Illinois at Chicago, Chicago, Illinois 60607, United States

Changying Xue — School of Bioengineering, Dalian University of Technology, 116024 Dalian, China

Yi Y. Zuo — Department of Mechanical Engineering, University of Hawaii at Manoa, Honolulu, Hawaii 96822, United States; orcid.org/0000-0002-3992-3238

Complete contact information is available at: https://pubs.acs.org/10.1021/acs.nanolett.3c02128

#### Notes

The authors declare no competing financial interest.

#### ACKNOWLEDGMENTS

This work was supported by the National Key Research and Development Program of China (2022YFC2304305), the National Natural Science Foundation of China (U22A20455 and 31870919), the Dalian Science and Technology Innovation Fund (2020JJ25CY015), and the Fundamental Research Funds for the Central Universities (DUT21ZD216, DUT22LAB601, and DUT22YG120).

#### REFERENCES

- (1) Lieleg, O.; Ribbeck, K. Biological Hydrogels as Selective Diffusion Barriers. *Trends Cell Biol.* **2011**, *21*, 543–551.
- (2) Fu, D.; Wang, M.; Yang, T.; Li, M.; Liang, Z.; Chen, C.; Zhang, L.; Xue, C.; Sun, B.; Mao, C. Self-Assembled Flagella Protein Nanofibers Induce Enhanced Mucosal Immunity. *Biomaterials* **2022**, 288, 121733.
- (3) Bandi, S. P.; Bhatnagar, S.; Venuganti, V. V. K. Advanced Materials for Drug Delivery across Mucosal Barriers. *Acta Biomater.* **2021**, *119*, 13–29.
- (4) Wu, L.; Shan, W.; Zhang, Z.; Huang, Y. Engineering Nanomaterials to Overcome the Mucosal Barrier by Modulating Surface Properties. *Adv. Drug Delivery Rev.* **2018**, *124*, 150–163.
- (5) Ensign, L. M.; Schneider, C.; Suk, J. S.; Cone, R.; Hanes, J. Mucus Penetrating Nanoparticles: Biophysical Tool and Method of Drug and Gene Delivery. *Adv. Mater.* **2012**, *24*, 3887–3894.
- (6) Li, Q.; Wen, C.; Yang, J.; Zhou, X.; Zhu, Y.; Zheng, J.; Cheng, G.; Bai, J.; Xu, T.; Ji, J.; Jiang, S.; Zhang, L.; Zhang, P. Zwitterionic Biomaterials. *Chem. Rev.* **2022**, *122*, 17073–17154.
- (7) Han, X.; Lu, Y.; Xie, J.; Zhang, E.; Zhu, H.; Du, H.; Wang, K.; Song, B.; Yang, C.; Shi, Y.; Cao, Z. Zwitterionic Micelles Efficiently Deliver Oral Insulin without Opening Tight Junctions. *Nat. Nanotechnol.* **2020**, *15*, 605–614.
- (8) Zheng, Y.; Xing, L.; Chen, L.; Zhou, R.; Wu, J.; Zhu, X.; Li, L.; Xiang, Y.; Wu, R.; Zhang, L.; Huang, Y. Tailored Elasticity Combined with Biomimetic Surface Promotes Nanoparticle Transcytosis to Overcome Mucosal Epithelial Barrier. *Biomaterials* **2020**, *262*, 120323.
- (9) Rao, R.; Liu, X.; Li, Y.; Tan, X.; Zhou, H.; Bai, X.; Yang, X.; Liu, W. Bioinspired Zwitterionic Polyphosphoester Modified Porous Silicon Nanoparticles for Efficient Oral Insulin Delivery. *Biomaterials Science* **2021**, *9*, 685–699.
- (10) Li, Y.; Ji, W.; Peng, H.; Zhao, R.; Zhang, T.; Lu, Z.; Yang, J.; Liu, R.; Zhang, X. Charge-Switchable Zwitterionic Polycarboxybetaine Particle as an Intestinal Permeation Enhancer for 454 Efficient Oral Insulin Delivery. *Theranostics* **2021**, *11*, 4452–4466.
- (11) Gao, Y.; He, Y.; Zhang, H.; Zhang, Y.; Gao, T.; Wang, J.-H.; Wang, S. Zwitterion-Functionalized Mesoporous Silica Nanoparticles for Enhancing Oral Delivery of Protein Drugs by Overcoming Multiple Gastrointestinal Barriers. *J. Colloid Interface Sci.* **2021**, 582, 364–375.
- (12) Shan, W.; Zhu, X.; Tao, W.; Cui, Y.; Liu, M.; Wu, L.; Li, L.; Zheng, Y.; Huang, Y. Enhanced Oral Delivery of Protein Drugs Using Zwitterion-Functionalized Nanoparticles to Overcome Both the Diffusion and Absorption Barriers. ACS Appl. Mater. Interfaces 2016, 8, 25444–25453.
- (13) Chen, Z. Surface Hydration and Antifouling Activity of Zwitterionic Polymers. *Langmuir* **2022**, *38*, 4483–4489.
- (14) Leng, C.; Han, X.; Shao, Q.; Zhu, Y.; Li, Y.; Jiang, S.; Chen, Z. In Situ Probing of the Surface Hydration of Zwitterionic Polymer Brushes: Structural and Environmental Effects. *J. Phys. Chem. C* **2014**, *118*, 15840–15845.
- (15) Yu, B.; Liu, J.; Liu, S.; Zhou, F. Pdop Layer Exhibiting Zwitterionicity: A Simple Electrochemical Interface for Governing Ion Permeability. *Chem. Commun.* **2010**, *46*, 5900–5902.
- (16) Feng, H.; Zhu, X.; Chen, R.; Liao, Q.; Ye, D.; Zhang, B.; Liu, J.; Liu, M.; Chen, G.; Wang, K. Ph Response of Zwitterionic Polydopamine Layer to Palladium Deposition in the Microchannel. *Chem. Eng. J.* 2019, 356, 282–291.
- (17) Alswieleh, A. M.; Cheng, N.; Canton, I.; Ustbas, B.; Xue, X.; Ladmiral, V.; Xia, S. J.; Ducker, R. E.; El Zubir, O.; Cartron, M. L.; Hunter, C. N.; Leggett, G. J.; Armes, S. P. Zwitterionic Poly(Amino Acid Methacrylate) Brushes. *J. Am. Chem. Soc.* **2014**, *136*, 9404–9413.
- (18) Zhang, Z.; Vaisocherová, H.; Cheng, G.; Yang, W.; Xue, H.; Jiang, S. Nonfouling Behavior of Polycarboxybetaine-Grafted Surfaces: Structural and Environmental Effects. *Biomacromolecules* **2008**, *9*, 2686–2692.
- (19) Murugan, P.; Ramar, P.; Mandal, A. B.; Samanta, D. Polymer Brush on Surface with Tunable Hydrophilicity Using Sam Formation of Zwitterionic 4-Vinylpyridine-Based Polymer. *New J. Chem.* **2018**, 42, 2513–2519.

- (20) Demirci, S.; Kinali-Demirci, S.; Caykara, T. Novel Ph-Responsive Mixed-Charge Copolymer Brushes Based on Carboxylic Acid and Quaternary Amine Monomers. *J. Polym. Sci., Part A: Polym. Chem.* **2013**, *51*, 1612–1619.
- (21) Lieleg, O.; Vladescu, I.; Ribbeck, K. Characterization of Particle Translocation through Mucin Hydrogels. *Biophys. J.* **2010**, *98*, 1782–1789.
- (22) Leal, J.; Smyth, H. D. C.; Ghosh, D. Physicochemical Properties of Mucus and Their Impact on Transmucosal Drug Delivery. *Int. J. Pharm.* **2017**, 532, 555–572.
- (23) McShane, D.; Davies, J. C.; Davies, M. G.; Bush, A.; Geddes, D. M.; Alton, E. W. Airway Surface Ph in Subjects with Cystic Fibrosis. *Eur. Respir. J.* **2003**, *21*, 37–42.
- (24) Avetisov, S.; Safonova, T. N.; Novikov, I. A.; Pateiuk, L. S.; Griboedova, I. G. [Ocular Surface Acidity and Buffering System (by Studying the Conjunctival Sac)]. *Vestnik Oftalmologii* **2014**, *130*, 5–10.
- (25) Ruiz-Pulido, G.; Medina, D. I. An Overview of Gastrointestinal Mucus Rheology under Different Ph Conditions and Introduction to Ph-Dependent Rheological Interactions with Plga and Chitosan Nanoparticles. Eur. J. Pharm. Biopharm. 2021, 159, 123–136.
- (26) Rajput, G. C.; Majmudar, F. D.; Patel, J.; Thakor, R. S.; Rajgor, N. B. Stomach-Specific Mucoadhesive Microsphere as a Controlled Drug Delivery System. *Syst. Rev. Pharm.* **2010**, *1*, 70–78.
- (27) das Neves, J.; Amiji, M.; Sarmento, B. Mucoadhesive Nanosystems for Vaginal Microbicide Development: Friend or Foe? *Wiley interdisciplinary reviews. Nanomedicine and nanobiotechnology* **2011**, *3*, 389–399.
- (28) Lai, S. K.; O'Hanlon, D. E.; Harrold, S.; Man, S. T.; Wang, Y.-Y.; Cone, R.; Hanes, J. Rapid Transport of Large Polymeric Nanoparticles in Fresh Undiluted Human Mucus. *Proc. Natl. Acad. Sci. U. S. A.* **2007**, *104*, 1482–1487.
- (29) Li, M.; Cheng, F.; Xue, C.; Wang, H.; Chen, C.; Du, Q.; Ge, D.; Sun, B. Surface Modification of Stöber Silica Nanoparticles with Controlled Moiety Densities Determines Their Cytotoxicity Profiles in Macrophages. *Langmuir* **2019**, *35*, 14688–14695.
- (30) Ruppel, S. S.; Liang, J. Tunable Properties of Polydopamine Nanoparticles and Coated Surfaces. *Langmuir* **2022**, *38*, 5020–5029.
- (31) Iler, R. K. The Chemistry of Silica: Solubility, Polymerization, Colloid and Surface Properties and Biochemistry of Silica; John Wiley and Sons: Chichester, U.K., 1979.
- (32) Liebscher, J.; Mrówczyński, R.; Scheidt, H. A.; Filip, C.; Hǎdade, N. D.; Turcu, R.; Bende, A.; Beck, S. Structure of Polydopamine: A Never-Ending Story? *Langmuir* **2013**, *29*, 10539–10548.
- (33) Zhan, G.; Zeng, H. C. Charge-Switchable Integrated Nanocatalysts for Substrate-Selective Degradation in Advanced Oxidation Processes. *Chem. Mater.* **2016**, *28*, 4572–4582.
- (34) Poinard, B.; Lam, S. A. E.; Neoh, K. G.; Kah, J. C. Y. Mucopenetration and Biocompatibility of Polydopamine Surfaces for Delivery in an Ex Vivo Porcine Bladder. *J. Controlled Release* **2019**, 300, 161–173.
- (35) Guo, Y.; Ma, Y.; Chen, X.; Li, M.; Ma, X.; Cheng, G.; Xue, C.; Zuo, Y. Y.; Sun, B. Mucus Penetration of Surface-Engineered Nanoparticles in Various Ph Microenvironments. *ACS Nano* **2023**, *17*, 2813–2828.
- (36) Hu, S.; Pei, X.; Duan, L.; Zhu, Z.; Liu, Y.; Chen, J.; Chen, T.; Ji, P.; Wan, Q.; Wang, J. A Mussel-Inspired Film for Adhesion to Wet Buccal Tissue and Efficient Buccal Drug Delivery. *Nat. Commun.* **2021**, 12, 1689.
- (37) Hu, S.; Yang, Z.; Wang, S.; Wang, L.; He, Q.; Tang, H.; Ji, P.; Chen, T. Zwitterionic Polydopamine Modified Nanoparticles as an Efficient Nanoplatform to Overcome Both the Mucus and Epithelial Barriers. *Chem. Eng. J.* **2022**, 428, 132107.
- (38) Poinard, B.; Kamaluddin, S.; Tan, A. Q. Q.; Neoh, K. G.; Kah, J. C. Y. Polydopamine Coating Enhances Mucopenetration and Cell Uptake of Nanoparticles. *ACS Appl. Mater. Interfaces* **2019**, *11*, 4777–4789.
- (39) Huck, B. C.; Hartwig, O.; Biehl, A.; Schwarzkopf, K.; Wagner, C.; Loretz, B.; Murgia, X.; Lehr, C.-M. Macro- and Microrheological

Properties of Mucus Surrogates in Comparison to Native Intestinal and Pulmonary Mucus. Biomacromolecules 2019, 20, 3504-3512.

- (40) Murgia, X.; Loretz, B.; Hartwig, O.; Hittinger, M.; Lehr, C.-M. The Role of Mucus on Drug Transport and Its Potential to Affect Therapeutic Outcomes. Adv. Drug Delivery Rev. 2018, 124, 82-97.
- (41) Song, D.; Cahn, D.; Duncan, G. A. Mucin Biopolymers and Their Barrier Function at Airway Surfaces. Langmuir 2020, 36, 12773–12783.
- (42) Kim, K.; Kim, K.; Ryu, J. H.; Lee, H. Chitosan-Catechol: A Polymer with Long-Lasting Mucoadhesive Properties. Biomaterials **2015**, *52*, 161–170.
- (43) Sriamornsak, P.; Wattanakorn, N.; Takeuchi, H. Study on the Mucoadhesion Mechanism of Pectin by Atomic Force Microscopy and Mucin-Particle Method. Carbohydr. Polym. 2010, 79, 54-59.
- (44) Cheng, Z.; Chen, X.; Zhai, D.; Gao, F.; Guo, T.; Li, W.; Hao, S.; Ji, J.; Wang, B. Development of Keratin Nanoparticles for Controlled Gastric Mucoadhesion and Drug Release. J. Nanobiotechnol. 2018, 16,
- (45) Witten, J.; Samad, T.; Ribbeck, K. Selective Permeability of Mucus Barriers. Curr. Opin. Biotechnol. 2018, 52, 124-133.
- (46) Amiji, M. M. Pyrene Fluorescence Study of Chitosan Self-Association in Aqueous Solution. Carbohydr. Polym. 1995, 26, 211-
- (47) Li, T.; Zhong, Q.; Zhao, B.; Lenaghan, S.; Wang, S.; Wu, T. Effect of Surface Charge Density on the Ice Recrystallization Inhibition Activity of Nanocelluloses. Carbohydr. Polym. 2020, 234, 115863.
- (48) Han, X.; Leng, C.; Shao, Q.; Jiang, S.; Chen, Z. Absolute Orientations of Water Molecules at Zwitterionic Polymer Interfaces and Interfacial Dynamics after Salt Exposure. Langmuir 2019, 35, 1327-1334.
- (49) Bansil, R.; Turner, B. S. Mucin Structure, Aggregation, Physiological Functions and Biomedical Applications. Curr. Opin. Colloid Interface Sci. 2006, 11, 164-170.
- (50) Lee, S.; Müller, M.; Rezwan, K.; Spencer, N. D. Porcine Gastric Mucin (Pgm) at the Water/Poly(Dimethylsiloxane) (Pdms) Interface: Influence of Ph and Ionic Strength on Its Conformation, Adsorption, and Aqueous Lubrication Properties. Langmuir 2005, 21, 8344-8353.
- (51) Maheshwari, R.; Dhathathreyan, A. Mucin at Solution/Air and Solid/Solution Interfaces. J. Colloid Interface Sci. 2006, 293, 263-269.
- (52) Cao, X.; Bansil, R.; Bhaskar, K. R.; Turner, B. S.; LaMont, J. T.; Niu, N.; Afdhal, N. H. Ph-Dependent Conformational Change of Gastric Mucin Leads to Sol-Gel Transition. Biophys. J. 1999, 76, 1250-1258.
- (53) Yu, G.; Liang, Z.; Yu, Z.; Li, M.; Yang, W.; Zhang, Y.; Zhao, Y.; Yang, C.; Xue, C.; Shi, L.; Sun, B. Engineering the Hydroxyl Content on Aluminum Oxyhydroxide Nanorod for Elucidating the Antigen Adsorption Behavior. npj Vaccines 2022, 7, 62.
- (54) De, M.; You, C.-C.; Srivastava, S.; Rotello, V. M. Biomimetic Interactions of Proteins with Functionalized Nanoparticles: A Thermodynamic Study. J. Am. Chem. Soc. 2007, 129, 10747-10753.
- (55) Wang, Q.; Chen, W.-Q.; Liu, X.-Y.; Liu, Y.; Jiang, F.-L. Thermodynamic Implications and Time Evolution of the Interactions of near-Infrared Pbs Quantum Dots with Human Serum Albumin. ACS Omega 2021, 6, 5569-5581.
- (56) Prozeller, D.; Morsbach, S.; Landfester, K. Isothermal Titration Calorimetry as a Complementary Method for Investigating Nanoparticle-Protein Interactions. Nanoscale 2019, 11, 19265-19273.
- (57) Huang, R.; Lau, B. L. T. Biomolecule-Nanoparticle Interactions: Elucidation of the Thermodynamics by Isothermal Titration Calorimetry. Biochimica et Biophysica Acta (BBA) - General Subjects **2016**, 1860, 945-956.
- (58) Hsein, H.; Garrait, G.; Beyssac, E.; Hoffart, V. Whey Protein Mucoadhesive Properties for Oral Drug Delivery: Mucin-Whey Protein Interaction and Mucoadhesive Bond Strength. Colloids Surf. B. Biointerfaces 2015, 136, 799-808.
- (59) Uthaiwat, P.; Priprem, A.; Puthongking, P.; Daduang, J.; Nukulkit, C.; Chio-Srichan, S.; Boonsiri, P.; Thapphasaraphong, S. Characteristic Evaluation of Gel Formulation Containing Niosomes of Melatonin or Its Derivative and Mucoadhesive Properties Using Atr-Ftir Spectroscopy. Polymers (Basel) 2021, 13, 1142.

- (60) McConnell, E. L.; Basit, A. W.; Murdan, S. Measurements of Rat and Mouse Gastrointestinal Ph, Fluid and Lymphoid Tissue, and Implications for in-Vivo Experiments. J. Pharm. Pharmacol. 2010, 60, 63 - 70.
- (61) Xu, Y.; Shrestha, N.; Préat, V.; Beloqui, A. An Overview of in Vitro, Ex Vivo and in Vivo Models for Studying the Transport of Drugs across Intestinal Barriers. Adv. Drug Deliv Rev. 2021, 175, 113795.
- (62) Leal, J.; Peng, X.; Liu, X.; Arasappan, D.; Wylie, D. C.; Schwartz, S. H.; Fullmer, J. J.; McWilliams, B. C.; Smyth, H. D. C.; Ghosh, D. Peptides as Surface Coatings of Nanoparticles That Penetrate Human Cystic Fibrosis Sputum and Uniformly Distribute in Vivo Following Pulmonary Delivery. J. Controlled Release 2020, 322, 457-469.
- (63) Cui, Q.; Le, T.-H.; Lin, Y.-J.; Miao, Y.-B.; Sung, I. T.; Tsai, W.-B.; Chan, H.-Y.; Lin, Z.-H.; Sung, H.-W. A Self-Powered Battery-Driven Drug Delivery Device That Can Function as a Micromotor and Galvanically Actuate Localized Payload Release. Nano Energy 2019, 66, 104120.

# NOTE ADDED AFTER ASAP PUBLICATION

This paper published post-ASAP on July 26, 2023 with a production error in references 10 and 11. The error was corrected and the paper reposted on July 27, 2023.

# **□** Recommended by ACS

# Increase Nebulization Stability of Lipid Nanoparticles by **Integrating a DNA Supramolecular Hydrogel**

Xunan Wei, Yuanchen Dong, et al.

MAY 19, 2023

ACS MACRO LETTERS

READ 2

# **Multifunctional Janus Nanoplatform for Efficiently Synergistic Theranostics of Rheumatoid Arthritis**

Yuvi Liu, Jian Dong, et al.

APRIL 21, 2023

ACS NANO

READ **C** 

# A Comparative Study of Ultrasmall Calcium Carbonate Nanoparticles for Targeting and Imaging Atherosclerotic **Plaque**

Lydia Martínez-Parra, Susana Carregal-Romero, et al.

JULY 03, 2023

ACS NANO

READ **C** 

**Temperature-Dependent Nanogel for Pesticide Smart** Delivery with Improved Foliar Dispersion and Bioactivity for **Efficient Control of Multiple Pests** 

Yue Shen, Yan Wang, et al.

DECEMBER 05, 2022

ACS NANO

RFAD 🗹

Get More Suggestions >